

The X-shaped radio galaxy 3C 223.1: A ‘double boomerang’ with anomalous spectral gradient

Gopal-Krishna^{1*} and Pratik Dabhade^{2**}

¹UM-DAE Centre for Excellence in Basic Sciences (CEBS), Vidyanagari, Mumbai - 400098, India

²Observatoire de Paris, LERMA, Collège de France, CNRS, PSL University, Sorbonne University, 75014, Paris, France

July 11, 2022

ABSTRACT

A comparison of the recent LOFAR 144 MHz map of the radio source 3C 223.1 (J094124.028+394441.95) with its VLA maps at 4.9 GHz and 8.3 GHz, made by us using the archival data, establishes this X-shaped radio galaxy (XRG) as the singularly robust case where the ‘wings’ exhibit a distinctly flatter radio spectrum than the primary lobes. The details of its anomalous spectral gradient are unravelled here with unprecedented precision. We also highlight the ‘double boomerang’ type radio morphology of this XRG. It is suggested that the peculiar spectral gradient in this XRG owes to particle acceleration associated with the rebounding of the collimated backflows of synchrotron plasma streaming in its two primary lobes, as they impinge upon and encounter the magnetic tension in the prominent dusty disk of the elliptical galaxy hosting this XRG. We also draw attention to an intriguing new morphological peculiarity of XRGs, namely a lateral offset observed between the (parallel) axes of the two primary radio lobes.

Key words. galaxies: jets – galaxies: active – galaxies: intergalactic medium – galaxies: groups:general – radio continuum: galaxies

1. Introduction

X-shaped radio galaxies (XRG) are a numerically small but enigmatic species in the zoo of radio galaxies, since their radio emission arises from not one, but two (mis-aligned) pairs of radio lobes of comparable extent (e.g. Leahy & Williams 1984; Capetti et al. 2002). Of these, the ‘primary’ (i.e., active) lobes often show a terminal hot spot which signifies an ongoing energy supply via bi-polar jets. In contrast, the secondary lobes (‘wings’) are usually diffuse and devoid of a terminal hot spot. Two major explanations have been advanced for this morphological dichotomy: (i) each wing is merely a continuation of the hydrodynamical ‘back flow’ in the primary lobe, which gets deflected due to buoyancy forces, upon impinging on an ellipsoidal hot interstellar medium (ISM) of the parent galaxy (Leahy & Williams 1984; Worrall et al. 1995; Hodges-Kluck et al. 2010), or (ii) the wings are relics of the lobe pair whose energy supply ceased as the twin-jets feeding them flipped over to a new direction due to merger of the jetted super-massive black hole (SMBH) with another SMBH, thus giving rise to the active lobes seen presently (Rottmann 2001; Zier & Biermann 2001). This possibility of spin-flip via SMBH merger and the consequent emission of gravity waves (Merritt & Ekers 2002) brought XRGs into the limelight about two decades ago, even though the first example of XRG (3C 315) has been known for nearly half a century (Högbom & Carlsson 1974).

Clearly, spectral index mapping as an indicator of the ages of different parts of XRGs is a key step towards un-

derstanding the origin of the XRG phenomenon. Early studies of XRG 3C 315 resulted in contradictory claims about spectral index gradients in this radio source (Högbom 1979; Alexander & Leahy 1987). The reported lack of spectral gradients (Högbom 1979) was intriguing, since in both above models of XRGs, the wings are identified as the repository of aged synchrotron plasma. Rottmann (2001) investigated this issue by comparing his single-dish (Effelsberg) images of 9 prominent XRGs at 10.5 GHz (beam $\sim 1.15'$) and 7 of them also at 32 GHz (beam $\sim 0.45'$), with the existing Westerbork telescope maps made below 1 GHz and VLA maps between 1 to 8 GHz. The use of high-frequency maps is advantageous for identifying regions of synchrotron ageing. Interestingly, for two XRGs in his sample, namely 3C 223.1 and 3C 403, Rottmann (2001) reported an anomalous spectral index distribution, with the wings exhibiting a flatter radio spectrum compared to the primary lobes. He also found these two sources to have the smallest spectral ages in his XRG sample. Dennett-Thorpe et al. (2002) confirmed a flatter spectrum for the wings in 3C 223.1, but found the spectral difference to be marginal ($\alpha_{\text{lobe}} - \alpha_{\text{wing}} \sim 0.08$). A similar ‘tendency’ was reported by Mack et al. (2005), based on their spectral index map (74 - 1400 MHz) with a $45''$ beam which could, however, barely resolve the wings. On the other hand, a distinctly flatter spectrum of the wings in 3C 223.1 was reported by Lal & Rao (2005), in spite of their using maps made at metre-wavelengths (240 - 610 MHz) where spectral steepening is expected to be less pronounced. These rather dissonant findings about the significance level of spectral flattening in the wings gave us the impetus to take a fresh look into the reported spectral peculiarity of this $z = 0.1075$ XRG.

* E-mail: gopaltani@gmail.com

** E-mail: pratik.dabhade@obspm.fr

We have taken advantage of the recently available LO-FAR maps of 3C 223.1 at 144 MHz with 6'' and 20'' beams (LoTSS-DR2¹; Shimwell et al. 2022), in conjunction with the VLA images at C-band and X-band, obtained by us from the NRAO VLA Archive Survey². These VLA D-array maps at C and X-bands have beamwidths of 14.2'' × 11.7'', and 8.2'' × 6.7'', respectively.

2. Spectral index mapping of the XRG 3C 223.1

The above mentioned LoTSS-DR2 map at 144 MHz was combined with the VLA maps at 4910 MHz and 8350 MHz, following the method given by Hoang et al. (2017), for generating the three-frequencies spectral index map with 20'' matched beam. These VLA D-array maps at 4.91 and 8.35 GHz essentially recover the entire radio structure of this XRG, since their integrated flux densities of 0.80 ± 0.04 Jy and 0.52 ± 0.03 Jy, respectively, are in full accord with the integrated spectrum (see Fig. 1b and Tab. 1).

This is consistent with the fact that even at 8.35 GHz, dense uv coverage of the VLA D-array data used here extends down to 35 m, which is enough to pick up the entire structure of this bright 2.0' radio source. Fig. 1 c-d display the derived spectral index and error maps, based on a combination of high sensitivity, resolution and frequency range (1 : 58) which is unmatched for this XRG. Spectral flattening is distinctly visible towards each wing. In the primary lobes, the northern and southern hot spots have $\alpha_{144}^{8350} = -0.70 \pm 0.04$ and -0.73 ± 0.04 , respectively and their associated (primary) lobes exhibit a spectral steepening by $\Delta\alpha \sim 0.1$. However, going further into the wings, the spectral gradient reverses sign and the spectrum turns markedly flatter along the ridge line, right up to the wing's edge. Interestingly, spectrum in certain parts of the wings is even flatter than it is at the hot spots. This confirms with a much higher precision and in much greater spatial detail the original result from Rottmann (2001) and is also consistent with the findings of Lal & Rao (2005). This point is further discussed in the next section.

Table 1: Integrated flux densities of 3C223.1 (Fig. 1b). Reference: 1) Present work, based on LoTSS-DR2 (Shimwell et al. 2022) & NVSS (Condon et al. 1998), 2) Kellermann et al. (1968), 3) Kellermann & Pauliny-Toth (1973), 4) Black et al. (1992), 5) Mack et al. (2005).

Frequency (MHz)	Flux (Jy)	Telescope	Beam	Ref
74	19.7±3.6	VLA-A	24''	5
144	9.7±0.9	LoFAR	20''	1
1400	2.0±0.1	VLA-C-D	45''	1
2695	1.23±0.04	NRAO-140ft	11.3' × 10.5'	2
4910	0.80±0.04	VLA-D	20''	4
8350	0.52±0.03	VLA-D	20''	4
10700	0.31±0.03	Effelsberg	2.85'	3

3. Discussion

The spectral index map presented in Fig. 1c clearly establishes XRG 3C 223.1 (J094124.028+394441.95) as the prime example of an XRG whose wings have a flatter radio spectrum than the primary lobes, thus challenging the currently popular models of XRGs, including the back-flow diversion

model mentioned in Sec. 1. A potentially useful hint for the origin of this anomalous spectral gradient comes from the recent MeerKAT observations of the XRG PKS 2014-55, dubbed as ‘double-boomerang’ XRG (dbXRG), which is hosted by a Seyfert 2 elliptical galaxy located in a poor group of galaxies at $z = 0.06063$ (Cotton et al. 2020 and references therein). Although this giant XRG is currently the leading exponent of the ‘double-boomerang’ morphology, a few other XRGs with similar appearance have been reported (e.g. Lal et al. 2019), including the prototypical XRG, 3C 315 itself (Högbom & Carlsson 1974), as well as the newly recognised case of XRG J1552+6534 whose LoTSS-DR2 image is presented in Fig. 3, resembling a ‘double crescent’. It may be noted that even for 3C 223.1, the existing 8.3 GHz VLA map with 2.5'' beam (Black et al. 1992) exhibits a turn-around of the back flow in each lobe, akin to the double-boomerang morphology (see, Fig. 2). The map also shows that the magnetic field is aligned with the edges of the radio lobes (see, also, Dennett-Thorpe et al. 2002). Probably due to the much greater relative spatial resolution available for the giant dbXRG PKS 2014-55, a sharp-edged faint radio cocoon of typical width ~ 50 kpc has been detected around both its lobe pairs and the two radio cocoons appear to almost touch each other near their apexes where the elliptical host galaxy is situated (Fig. 5 in Cotton et al. 2020). The cocoons appear to act as a sheath around the backflow both before and after its deflection. However, due to their faintness, the magnetic field geometry inside the radio cocoons is essentially unknown. Although, the exceptionally high relative spatial resolution afforded by the giant size of that dbXRG is not yet reachable for other dbXRGs, it seems reasonable to expect that the backflows in them, too, are surrounded by similar protective radio cocoons.

In the case of 3C 223.1, too, the two boomerangs are seen to approach each other to within $\sim 2''$ (~ 4.3 kpc), near the location of the host elliptical galaxy which is known to possess a conspicuous dusty disk extending across the stellar body of the optical galaxy (Fig. 1a, Fig. 2), at a position angle of $\sim 40^\circ$. The dusty disk was detected in a *Hubble Space Telescope* snapshot survey of radio galaxies (de Koff et al. 1996). This disk of large extent and right orientation may well be playing a significant role in blocking and deflecting the hydrodynamic backflow streaming through the two primary lobes. Compression of the magnetic field of the disk (and, possibly, of its synchrotron halo) by the impact of the collimated backflow could be contributing to the powerful push needed to transform the obliquely incident backflow into a boomerang shape. Post-rebound, the backflow propagation is guided by the steepest pressure gradient in the ISM of the host galaxy, as envisioned in Leahy & Williams (1984). A similar magnetic rebound may have contributed to the formation of the classic double boomerang in the giant dbXRG PKS 2014-55 where the backflow has been posited to impinge upon an ellipsoidal gaseous interstellar medium (ISM) of the host galaxy, with a required extent of ~ 150 kpc (Cotton et al. 2020). We note that even in this elliptical Seyfert-2 galaxy, a nearly edge-on dusty disk has been detected which too is oriented nearly along the symmetry plane of the double boomerang (Abbott et al. 2018; Cotton et al. 2020). However, in order to effectively contribute to the backflow rebounding observed in this giant XRG, the gaseous disk would have to be an order-of-magnitude larger than its detected extent of about 12 kpc. Such a possibility is not ruled out, however. Sen-

¹ https://lofar-surveys.org/dr2_release.html

² <http://www.vla.nrao.edu/astro/nvas/>

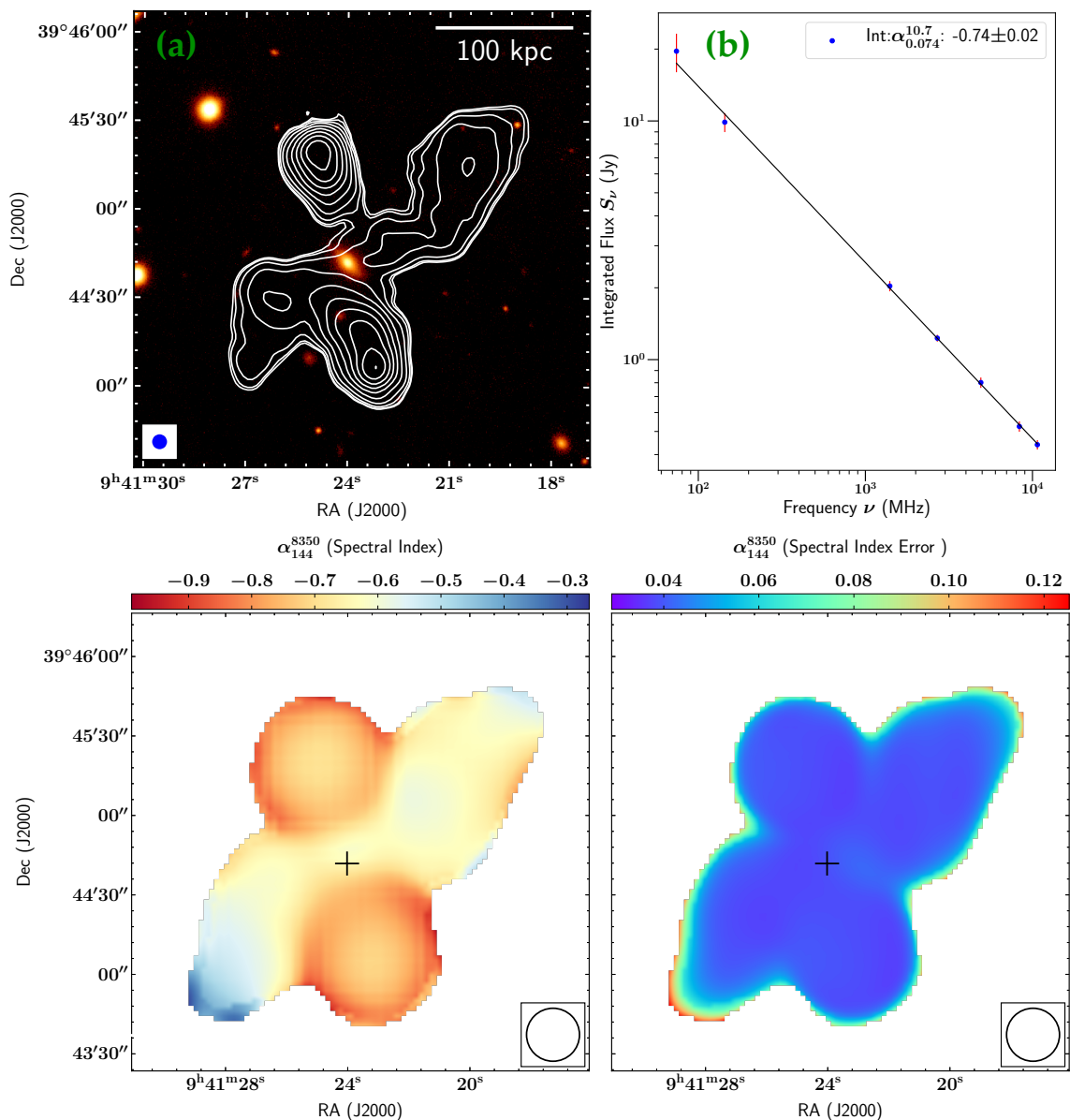


Fig. 1: (a): 3C223.1 LoTSS DR2 144 MHz radio contours (levels: 0.0085, 0.0097, 0.0134, 0.0213, 0.0384, 0.0754, 0.1549, 0.3263, 0.6955, and 1.4909 Jy beam $^{-1}$) of the $6''$ map overlaid on PanSTARRS r band image. (b): Integrated spectral index fit from 144 to 10700 MHz. (c): Three frequencies (144, 4910, and 8350 MHz) spectral index map and error map (d) of 3C223.1. The beam of $20'' \times 20''$ is shown at the bottom right corner. The host galaxy location is shown by the black marker.

sitive HI imaging of non-cluster early-type galaxies have revealed cases in which an HI disk extends over several tens of kpc, probably acquired from one or more approaching gas-rich galaxies, and such HI disks are prone to having kpc-scale central disks of dusty molecular gas (Serra et al. 2012; Yildiz et al. 2020).

Here, it is pertinent to recall an independent evidence for the role of magnetic tension, that has emerged from recent MeerKAT observations of the radio galaxy MRC 0600-399 in Abell 3376, followed-up with numerical simulations. Based on these, Chibueze et al. (2021) have argued that even the observed sharp bending of the relatively powerful jets of this Wide-Angle-Tail (WAT) radio galaxy has taken place due to the jets encountering the tension of a compressed layer of external magnetic field. More generally, the backflowing synchrotron plasma of a lobe could

also be diverted upon hitting a flattened gaseous structures, like a sheet or filament of the cosmic web, as recently proposed for the case of the giant radio galaxy GRG 0503-286 (Dabhade & Gopal-Krishna 2022, see also, Gopal-Krishna & Wiita 2009). A spectacular example of a flattened gaseous obstruction between the two lobes can be seen in the recent LoTSS-DR2 image of a large XRG (J0941+3227 of size ~ 0.6 Mpc), whose lobes appear separated by a ‘linear’ gap of average width ~ 25 kpc (Fig. 3a).

3.1. Clues to the flatter radio spectrum of the wings

In this section we summarise some observational clues bearing on the question of flatter radio spectrum of XRG wings (compared to the primary lobes), for which 3C 223.1 is demonstrated here to be a proto-type. In this dbXRG, the

Table 2: Coordinates of the host galaxies of 3 spectacular XRGs selected by us from LoTSS-DR2 (Fig. 3). The redshift (z), taken from the Sloan Digital Sky Survey (SDSS; York et al. 2000), is spectroscopic for J0941+3227 and photometric for J1328+5654. The sizes refer to the separation between the two hotspots (in the primary lobes). S_{144} is the integrated flux density at 144 MHz (LoTSS-DR2) and P_{144} the corresponding total radio luminosity. σ_{map} is the rms noise in the maps (Fig. 3). Throughout this paper we have adopted a flat cosmology with parameters $\Omega_m = 0.27$, and a Hubble constant of $H_0 = 71 \text{ km s}^{-1} \text{ Mpc}^{-1}$.

Source	R.A. (J2000)	Dec (J2000)	z	Size (")	Size (kpc)	S_{144} (Jy)	P_{144} ($\times 10^{26} \text{ W Hz}^{-1}$)	σ_{map} ($\mu\text{Jy beam}^{-1}$)
J0941+3227	09:41:46.10	+32:27:18.64	0.45261 \pm 0.00005	110	634	0.90 \pm 0.09	6.0	103
J1328+5654	13:28:31.82	+56:54:59.41	0.651 \pm 0.073	61	427	0.34 \pm 0.03	5.2	65
J1552+6534	15:52:06.34	+65:34:24.57	-	128	-	0.25 \pm 0.03	-	91

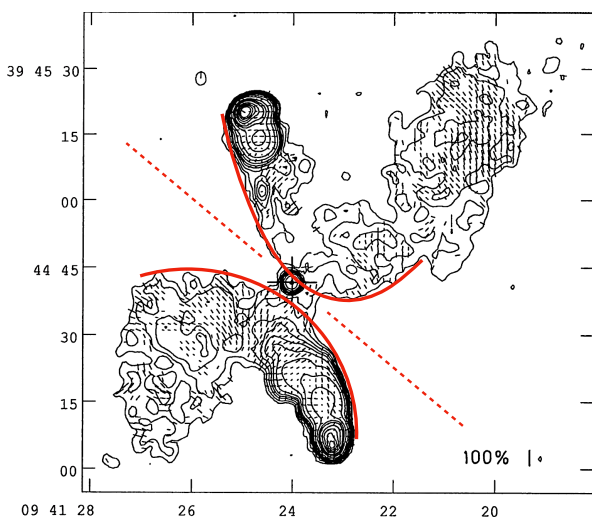


Fig. 2: Figure 4b from Black et al. (1992), where VLA 8 GHz 2.5'' image contours of 3C223.1 are shown with polarisation vectors. The contours are drawn at (-4,4,6,9,12,15,20,30,50,100,150,200,300,400,500, and 600) $\times 55 \mu\text{Jy beam}^{-1}$ (rms or σ_I). For the polarized intensity, the σ_P is $\sim 36 \mu\text{Jy beam}^{-1}$ and the vectors are drawn only at regions which have a surface-brightness $> 4\sigma_I$. We have marked outline of the 'double boomerang' in red colour along with the dashed line showing 40° position angle of the disk of the host galaxy (Fig. 1a).

clear reversal of radio spectral gradient following the deflection of the backflow into the wings (Sec. 2) stands in sharp contrast to the monotonous spectral steepening along the backflow, which is typical of edge-brightened double radio sources. We propose that the spectral flattening observed towards the wings in 3C 223.1 is linked to particle acceleration (or re-acceleration) during the process of rebounding of the backflow. Plausibly, this could occur as the backflow impinges upon the disk (and its likely synchrotron halo) and encounters the tension of their magnetic field lines compressed by the impact of the backflow. We may recall that in afore-mentioned both dbXRG PKS 2014-55 (Cotton et al. 2020) and the cluster radio source MRC 0600-399 (Chibueze et al. 2021), localised regions of enhanced radio emission accompanied by spectral flattening, have actually been observed near the areas where a powerful collimated flow of the synchrotron plasma (jet, or backflow) undergoes a sharp bending, or rebound. Such patches of flatter radio spectrum could either dilute, or mask the effect of spectral steepening in the ageing synchrotron plasma deflected into the XRG wings, or, in the extreme, even cause spectral flattening in the wings. Recent MHD simulations, reported in (Chibueze et al. 2021) have shown that when

a jet-flow encounters the tension of magnetic field lines in a compressed layer, an efficient conversion of the magnetic energy into relativistic particles via magnetic reconnection can occur and the relativistic particles, accelerated in situ, get transported along the deflected stream of synchrotron plasma (see, also, Giri et al. 2022). A similar process may be occurring at a significant level in the XRGs whose wings do not show spectral steepening, or even exhibit a spectral flattening, e.g., the rare case of XRG 3C 223.1. In view of this, it would be desirable to extend spectral index mapping to the several other XRGs which are candidates for wings having flatter radio spectra compared to the primary lobes, based on their metre wavelength imaging observations (Lal et al. 2019). It is important to extend their spectral mapping to centimetre wavelengths where spectral steepening due to synchrotron losses should be more pronounced. Also, it would be instructive to look for signs of spectral flattening in regions where the jet flow appears to undergo a deflection upon colliding with an obstruction like a galaxy shell. This possibility seems particularly relevant to the XRGs in which the wings take off sharply from the primary lobes at large distances ($\gg 10 \text{ kpc}$) from the parent galaxy, i.e., well beyond the likely interstellar medium of the parent galaxy (Gopal-Krishna et al. 2012; Joshi et al. 2019). Observational evidence for jet-shell interactions (Gopal-Krishna & Chitra 1983) has been reported for the nearest radio galaxy Centaurus A (Gopal-Krishna & Saripalli 1984; Gopal-Krishna & Wiita 2010).

3.2. A new kind of lobe symmetry in XRGs

Conceptually, the most straight-forward explanation for XRGs, perhaps inspired by the XRGs whose wings do not exhibit a steeper radio spectrum compared to the primary lobes, is that the central engine consists of a close binary of SMBH (see, Begelman et al. 1980), each of which produces its own pair of lobes (Lal & Rao 2005; Lal et al. 2019). However, several observations question the general applicability of this model, including the ubiquitous absence (i) of parsec-scale nuclear radio jets pointing towards the wings, and (ii) of terminal hot spots in the wings (see, Gopal-Krishna et al. 2012 for a review of the models of XRGs). Another challenge to this hypothesis stems from the detection of a lateral offset between the ridge-lines of the two wings in some well-mapped XRGs (Gopal-Krishna et al. 2003). Note that such an offset is problematic even for the basic spin-flip model (Sec. 1), however that model can be reconciled in case the wings arise due to bending of the twin-jets by the ISM of the host galaxy, which has been set in rotation during the orbital infall of a merging galaxy (Gopal-Krishna et al. 2003).

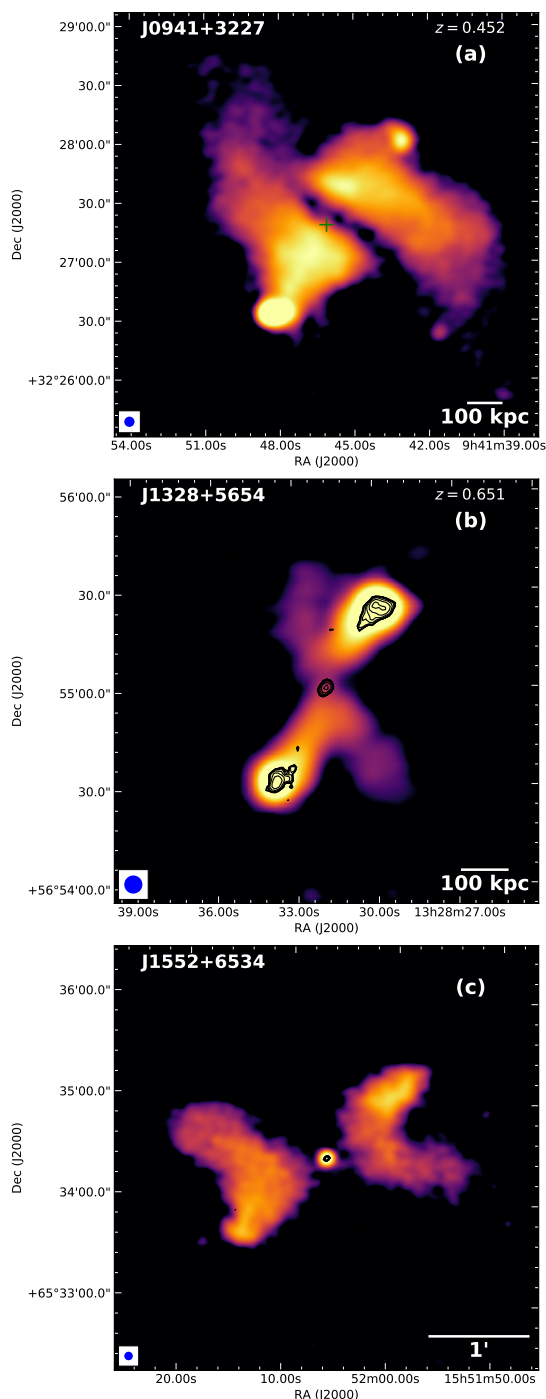


Fig. 3: Three spectacular XRGs culled by us from LoTSS-DR2: 6'' LoTSS 144 MHz images overlaid with VLASS 2.5'' contours, where only the radio emission greater than 3σ is shown. More details in Tab. 2. For J0941+3227 radio core coincident (not shown here) with the host galaxy is quite faint and is detected at 1σ in both FIRST and VLASS and is marked with '+' symbol in panel a.

Here, we would like to draw attention to a new kind of morphological peculiarity, namely a lateral offset between the pair of *primary* radio lobes which extend parallel to each other. A case of XRG (J1328+5654) exemplifying such an anomalous morphology is shown in Fig. 3b (LoFAR image and contours from the 3 GHz Very Large Array Sky Survey (VLASS; Lacy et al. 2020)). Such a morphology of the

primary lobes is puzzling, since they are widely believed to be directly fed by the bipolar jets emanating from the nucleus, unlike the wings (see, e.g., Cotton et al. 2020 and references therein). Unfortunately, the existing radio maps of this XRG lack the spatial resolution and sensitivity to trace the detailed trajectories of its jets, from the nucleus to the terminal hot spots seen in the primary lobes. It would be instructive to obtain this vital information through sensitive, high-resolution radio imaging in order to unravel how the bipolar jets in such XRGs undergo bending and how the backflows in the two lobes remain parallel to each other, while being laterally offset.

4. Conclusions

Taking advantage of the recent availability of the LoTSS-DR2 map of the X-shaped radio galaxy (XRG) 3C 223.1 at 144 MHz and using its archival VLA observations at 4.9 GHz and 8.4 GHz, we have mapped the radio spectral index distribution across this XRG with unprecedented precision and spatial detail. This firmly establishes it as a prime example of an XRG in which the radio wings exhibit a distinctly flatter spectrum than the primary lobes, setting aside the debate over the level of this spectral anomaly. Evidence is also presented in support of this XRG having a 'double boomerang' type radio morphology. Based on existing observational clues, we suggest that the flatter spectrum of the wings in this XRG manifests an extreme case of in-situ acceleration/energisation of relativistic particles as the collimated hydrodynamical backflow of synchrotron plasma in the primary lobes impinges obliquely upon the prominent gaseous disk (and its likely synchrotron plasma halo) within the host galaxy and rebounds due to the tension of its magnetic field lines which are compressed by the impact of the collimated backflows from opposite sides. Lastly, we have drawn attention to a new and intriguing morphological symmetry whereby the two primary lobes of an XRG, although parallel to each other, have a distinct lateral offset. Explaining this morphological anomaly appears more challenging than a similar morphological pattern found for the wings in several XRGs.

Acknowledgements

GK acknowledges a Senior Scientist fellowship of the Indian National Science Academy. We would like to dedicate this work to late Prof. S.M. Chitre who, together with one of the authors (GK) introduced the concept of jet-shell interactions in radio galaxies (Gopal-Krishna & Chitre 1983). The acknowledgment for LoTSS data usage can be found at <https://lofar-surveys.org/credits.html>. The VLA archival data was obtained via the NRAO VLA Archive Survey, (c) AUI/NRAO. We acknowledge that this work has made use of APLPY (Robitaille & Bressert 2012).

References

- Abbott, T. M. C., Abdalla, F. B., Allam, S., et al. 2018, ApJS, 239, 18 2
- Alexander, P. & Leahy, J. P. 1987, MNRAS, 225, 1 1
- Begelman, M. C., Blandford, R. D., & Rees, M. J. 1980, Nature, 287, 307 4
- Black, A. R. S., Baum, S. A., Leahy, J. P., et al. 1992, MNRAS, 256, 186 2, 4
- Capetti, A., Zamfir, S., Rossi, P., et al. 2002, A&A, 394, 39 1

- Chibueze, J. O., Sakemi, H., Ohmura, T., et al. 2021, *Nature*, 593, 47
3, 4
- Condon, J. J., Cotton, W. D., Greisen, E. W., et al. 1998, *AJ*, 115, 1693 2
- Cotton, W. D., Thorat, K., Condon, J. J., et al. 2020, *MNRAS*, 495, 1271 2, 4, 5
- Dabhade, P. & Gopal-Krishna. 2022, *A&A*, 660, L10 3
- de Koff, S., Baum, S. A., Sparks, W. B., et al. 1996, *ApJS*, 107, 621 2
- Dennett-Thorpe, J., Scheuer, P. A. G., Laing, R. A., et al. 2002, *MNRAS*, 330, 609 1, 2
- Giri, G., Vaidya, B., Rossi, P., et al. 2022, *A&A*, 662, A5 4
- Gopal-Krishna, Biermann, P. L., Gergely, L. Á., & Wiita, P. J. 2012, *Research in Astronomy and Astrophysics*, 12, 127 4
- Gopal-Krishna, Biermann, P. L., & Wiita, P. J. 2003, *ApJ*, 594, L103 4
- Gopal-Krishna & Chitre, S. M. 1983, *Nature*, 303, 217 4, 5
- Gopal-Krishna & Saripalli, L. 1984, *A&A*, 141, 61 4
- Gopal-Krishna & Wiita, P. J. 2009, *New A*, 14, 51 3
- Gopal-Krishna & Wiita, P. J. 2010, *New A*, 15, 96 4
- Hoang, D. N., Shimwell, T. W., Stroe, A., et al. 2017, *MNRAS*, 471, 1107 2
- Hodges-Kluck, E. J., Reynolds, C. S., Cheung, C. C., & Miller, M. C. 2010, *ApJ*, 710, 1205 1
- Högbom, J. A. 1979, *A&AS*, 36, 173 1
- Högbom, J. A. & Carlsson, I. 1974, *A&A*, 34, 341 1, 2
- Joshi, R., Krishna, G., Yang, X., et al. 2019, *ApJ*, 887, 266 4
- Kellermann, K. I. & Pauliny-Toth, I. I. K. 1973, *AJ*, 78, 828 2
- Kellermann, K. I., Pauliny-Toth, I. I. K., & Tyler, W. C. 1968, *AJ*, 73, 298 2
- Lacy, M., Baum, S. A., Chandler, C. J., et al. 2020, *PASP*, 132, 035001 5
- Lal, D. V. & Rao, A. P. 2005, *MNRAS*, 356, 232 1, 2, 4
- Lal, D. V., Sebastian, B., Cheung, C. C., & Pramesh Rao, A. 2019, *AJ*, 157, 195 2, 4
- Leahy, J. P. & Williams, A. G. 1984, *MNRAS*, 210, 929 1, 2
- Mack, K. H., Vigotti, M., Gregorini, L., et al. 2005, *A&A*, 435, 863 1, 2
- Merritt, D. & Ekers, R. D. 2002, *Science*, 297, 1310 1
- Robitaille, T. & Bressert, E. 2012, *APLpy: Astronomical Plotting Library in Python* 5
- Rottmann, H. 2001, PhD thesis, - 1, 2
- Serra, P., Oosterloo, T., Morganti, R., et al. 2012, *MNRAS*, 422, 1835 3
- Shimwell, T. W., Hardcastle, M. J., Tasse, C., et al. 2022, *A&A*, 659, A1 2
- Worrall, D. M., Birkinshaw, M., & Cameron, R. A. 1995, *ApJ*, 449, 93 1
- Yıldız, M. K., Peletier, R. F., Duc, P. A., & Serra, P. 2020, *A&A*, 636, A8 3
- York, D. G., Adelman, J., Anderson, Jr., J. E., et al. 2000, *AJ*, 120, 1579 4
- Zier, C. & Biermann, P. L. 2001, *A&A*, 377, 23 1